

λ -Reachability: Geometric-Horizon Safety Bellman Equations for Humanoid Safety

Rui Chen
Robotics Institute
Carnegie Mellon University
United States
ruic3@andrew.cmu.edu

Shangtao Li
Mechanical Engineering
Carnegie Mellon University
United States
shangtal@andrew.cmu.edu

Yifan Sun
Robotics Institute
Carnegie Mellon University
United States
yifansu@andrew.cmu.edu

Changliu Liu
Robotics Institute
Carnegie Mellon University
United States
cliu6@andrew.cmu.edu

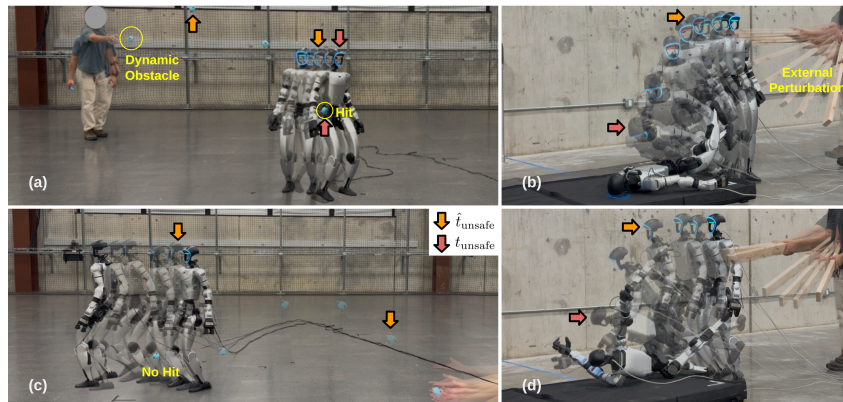


Figure 1: Safety value inference on hardware. A safety value V^π is learned to predict the state-wise worst-over-future safety signal ℓ , which models collision avoidance in task (a,c) and stable locomotion in task (b,d). The frame \hat{t}_{unsafe} when V^π predicts the first non-recoverable state (orange) and frame t_{unsafe} when the actual unsafe condition occurs (red) are both marked. The gap between \hat{t}_{unsafe} and t_{unsafe} is the predictive horizon of V^π for unsafe states. The headlight turns red at \hat{t}_{unsafe} when V^π predicts future safety violations.

Abstract: We introduce λ -Reachability, a scalable approach to Hamilton–Jacobi safety analysis for high-dimensional robotic systems. Unlike prior discounted formulations that rely on fixed one-step Bellman updates, λ -Reachability employs a *stochastic multi-step estimator* of the safety value, using a geometrically distributed rollout horizon together with a randomly absorbed terminal. Conceptually analogous to $\text{TD}(\lambda)$, λ -Reachability interpolates between local self-consistency updates and long-horizon max-over-trajectory safety targets via an interpretable horizon-control parameter. Unlike $\text{TD}(\lambda)$, where the terminal value is always incorporated in learning targets, the terminal safety value in λ -Reachability is only used at a probability controlled by parameter δ . We formally show that for $\delta < 1$, the update induces a contraction mapping that allows temporal-difference learning; as $\lambda \rightarrow 1$, the estimator recovers the undiscounted reachability objective. We apply λ -Reachability to high-dimensional safety learning problems with both simulated and real humanoid robots under balance and collision avoidance constraints. Experimental results demonstrate that λ -Reachability significantly improves both safe-set boundary classification and safety margin estimation compared to single-step temporal-difference baselines.

Keywords: Reachability Analysis, Reinforcement Learning, Humanoids

1 Introduction

Robots operating in the real world must reason about *persistent* safety: whether a policy will ever violate constraints, and how close it is to doing so. A common formalization uses an instantaneous safety signal, with its positivity indicating a violation, and defines a policy’s safety value as the worst future signal. Hence, the safety value certifies safety for all future time, with the sign indicating whether persistent safety is reachable and the magnitude acting as a safety margin. This worst-over-time notion is widely used as the foundational quantity for safety assessment [1].

Based on the safety assessment, a wide range of work focuses on *safe control*: producing actions that comply with safety constraints. Safe set algorithms (SSA) [2, 3] and control barrier functions (CBF) [4, 5] provide an optimization-based framework to enforce forward invariance within a safe set while retaining task performance. Hamilton-Jacobi (HJ) reachability-based methods [6, 1] recover the safety value by solving a variational inequality via dynamic programming. Those safe control approaches have been applied to real-world applications such as quadruped navigation [7, 8], collaborative manipulation [9], and autonomous driving [10]. To ultimately achieve safe control, the correctness of the safety value—both the sign indicating safety and the magnitude encoding safety margin—is an essential prerequisite, as it directly quantifies the safety performance. Only with accurate safety values, one is able to derive appropriate safe control operations, such as activating failure-recovery policies based on safety margins [11] and applying safe control constraints based on value gradients [12, 8]. Hence, this work focuses on acquiring accurate safety values for policies as a critical step in safety analysis and control.

Prior work that explicitly *synthesizes* or *learns* the underlying safety value with formal structure is often limited to relatively low-dimensional state descriptions. Safety Index Synthesis constructs a safety index by solving sum-of-squares (SOS) programs [13, 12, 14], but SOS formulations rely on semi-definite optimization whose size grows rapidly with state dimension and polynomial degree, leading to poor scalability [15]. Neural CBF learning methods aim to fit barrier functions from data [16], but unlike SOS- or PDE-based constructions whose constraints hold by design, learned neural barrier functions must satisfy barrier inequalities over a continuous state space; since training typically enforces these conditions only on sampled states, additional verification is required to establish safety guarantees [17, 18]. Similarly, HJ reachability computes a viscosity solution of the HJ (variational inequality) PDEs on a grid. However, standard solvers suffer from the curse of dimensionality—memory and computation scale exponentially with state dimension [19, 20]. These limitations are calling for new methods to learn safety value functions that can operate directly in high-dimensional robotic and perceptual representations.

To address the issue of high dimensionality, several works reformulate safety problems through *discounted* safety Bellman operators that admit contraction properties. This enables the use of reinforcement learning techniques, such as TD/Q-learning with function approximation [21, 22], to learn safety values from data. Ganai et al. [23] learns reachability estimators to support safe policy optimization, while Ganai et al. [1] summarizes the growing connections between HJ reachability and reinforcement learning. Notably, all existing works build on the safety Bellman equation with a one-step bootstrapped value target. In high-dimensional settings with rich perception (e.g., height maps) and complex environment dynamics, one-step bootstrapping can be unstable since approximation errors can be propagated through noisy transitions. The value learning can also be slow, since future safety information propagates by only one step per update. To avoid these drawbacks, one may consider removing bootstrapping entirely and learning from Monte Carlo-style targets instead. However, that requires full task trajectories, which can be costly to collect in high-dimensional real-world environments. It is also desirable to learn safety values while the system is in operation, instead of waiting for full rollouts which defers learning. In summary, we aim to efficiently learn safety value functions that accurately identify feasible boundaries and estimate safety margins, even from partial trajectory data.

Motivated by these challenges, we propose λ -*Reachability*, a TD(λ)-style approach [24] for safety value learning that replaces sensitive one-step backups with a geometric mixture of multi-step max

targets. By sampling a random rollout horizon and backing up the maximum observed safety signal over that horizon, λ -Reachability interpolates smoothly between short-horizon bootstrapping and Monte Carlo max targets, while providing an explicit knob (λ) that controls the effective look-ahead horizon. Instead of deterministically bootstrapping from the current safety value estimate, we do so only with a probability δ^n that decreases as the look-ahead horizon n extends. We formally prove that the resulting stochastic multi-step safety Bellman equation induces a contraction mapping when $\delta < 1$, thereby allowing temporal-difference solutions and recovering the undiscounted safety value in expectation as $\lambda \rightarrow 1$. We also interpret our approach as a connection between CBF and HJ-based approaches in terms of safety value learning. Finally, λ -Reachability is applied to high-dimensional robotic tasks using perceptual observations to recover safety values for balance and collision-avoidance constraints. Results in both simulations and on physical hardware show improved boundary and margin accuracy compared to one-step baselines.

2 Background

2.1 Safety Value Functions for Control Policies

Let $x \in \mathcal{X}$ be the system state and $u \in \mathcal{U}$ the control. During operation, the system should never enter unsafe states such as collisions and off-balance poses. We assume that such a constraint is specified through a *safety signal* $\ell : \mathcal{X} \rightarrow \mathbb{R}$, which defines a safe set we wish the system to stay in $\mathcal{X}_S := \{x \in \mathcal{X} \mid \ell(x) \leq 0\}$. Given a control policy $\pi : \mathcal{X} \rightarrow \mathcal{U}$, let τ_x^π denote the infinite-horizon state trajectory induced by π starting from x . If $\ell(\tau_x^\pi(t)) \leq 0$ for all t , τ_x^π is safe and the policy induces a forward invariant set [13] within \mathcal{X}_S . This work aims to synthesize a safety value function $V^\pi : \mathcal{X} \rightarrow \mathbb{R}$ that quantifies the future safety performance of π for any $x \in \mathcal{X}$, defined as

$$V^\pi(x_t) := \sup_{k \geq t} \ell(x_k) \quad (1)$$

It follows that $\{x \mid V^\pi(x) \leq 0\}$ is a forward invariant set within \mathcal{X}_S . By definition, (1) also satisfies the *safety Bellman equation*:

$$V^\pi(x) = \max\{\ell(x), V^\pi(f(x, \pi(x)))\} \quad (2)$$

2.2 The Discounted Safety Bellman Equation

Exact synthesis of the value function (1) has proven intractable for higher dimension problems either by Sum-of-Square programming [25, 13] or solving Hamilton- Jacobi-Bellman variational inequality [1]. Unlike standard reward-based Bellman equations, (2) does not induce a contraction mapping, which makes it unsuitable to derive a learning target directly [21]. To address this issue, Fisac et al. [21] introduces a γ -discounted formulation of the safety objective. For a discount factor $\gamma \in (0, 1)$, the *discounted safety Bellman equation* is defined as

$$V^\pi(x) = (1 - \gamma)\ell(x) + \gamma \max\{\ell(x), V^\pi(f(x, \pi(x)))\} \quad (3)$$

where γ can be interpreted as an episode continuing probability. This equation induces a contraction mapping under the supremum norm and admits a unique fixed point. Moreover, as $\gamma \rightarrow 1$, the solution V^π to (3) recovers the original undiscounted safety value in (1). Concretely, the learning is carried out by regressing $V^\pi(x_t)$ towards sampled targets y_t :

$$V_{k+1}^\pi(x_t) = V_k^\pi(x_t) + \alpha [y_t - V_k^\pi(x_t)] \quad (4)$$

where k is the training step and α is the learning rate. The target y_t is given by

$$y_t = (1 - \gamma)\ell_t + \gamma \max\{\ell_t, V_k^\pi(x_{t+1})\}, \quad (5)$$

with γ annealed to 1 during training. Hence, (3) is suitable for being used with temporal-difference techniques to provide a tractable way to synthesize safety value functions [21].

3 Stochastic Multi-step Safety Bellman Equation

3.1 Unifying Max Backups with Variable Horizon

Notice that the original safety objective in (1) is defined over an infinite horizon, whereas the update rule in (4) relies on a one-step bootstrap target at the successor state x_{t+1} . As a result, the regression target y_t is strongly influenced by the current approximation of $V^\pi(x_{t+1})$, which is typically inaccurate during early stages of training. This induces substantial bias in the learning signal and can lead to error propagation through repeated bootstrapping. Moreover, such myopic updates are inefficient at propagating safety information backward in time when unsafe events occur many steps after t . Similar limitations of one-step updates are well documented in the reinforcement learning literature for classic one-step temporal-difference (TD) methods [24].

At the opposite end of the spectrum, Monte-Carlo methods avoid bootstrapping altogether by constructing targets directly from fully observed trajectories. In the context of safety value learning, this corresponds to the target $y_t = \max\{\ell_t, \ell_{t+1}, \dots, \ell_T\}$ where T denotes the terminal time step. Monte-Carlo targets are unbiased with respect to the infinite-horizon objective (1) and provide accurate supervision when full trajectories are available. However, they typically exhibit high variance, require complete rollouts, and cannot always be computed until termination. These properties make Monte-Carlo supervision impractical for high-dimensional systems and incompatible with online learning settings, where only partial trajectory segments may be accessible.

Motivated by the complementary strengths and weaknesses of one-step bootstrapping and Monte-Carlo evaluation, our core contribution is to unify learning from max targets with different bootstrap horizons for safety value functions. Specifically, we propose a variant of safety Bellman equation with a geometric stopping horizon and stochastic terminal absorption. The equation smoothly interpolates between short-horizon bootstrapping and long-horizon Monte-Carlo supervision. Specifically, given state x_t , a continuation probability $\lambda \in [0, 1)$ and a terminal survival constant $\delta \in [0, 1)$, we define the following *stochastic multi-step safety Bellman equation*

$$V^\pi(x_t) = \mathbb{E}_{n,s|x_t} \left[\max \{ \ell_t, \ell_{t+1}, \dots, \ell_{t+n-1}, b_t^{(n)} \} \right] \quad (6)$$

where the stochastic bootstrapped value is given by

$$b_t^{(n)} := sV^\pi(x_{t+n}) + (1-s)v_{\text{term}}. \quad (7)$$

The stopping step $n \geq 1$ follows a geometric distribution $n \sim \text{Geom}(1 - \lambda)$ given by

$$\mathbb{P}(n = k) = (1 - \lambda)\lambda^{k-1}, \quad k \in \mathbb{N}. \quad (8)$$

The terminal survival event $s \sim \text{Bernoulli}(\delta^n)$ bootstraps on the current value estimation with a probability that decreases as the horizon grows. v_{term} is a lower bound of ℓ so that when $s = 0$, the bootstrapped value at $t + n$ is effectively ignored. Importantly, although (6) does not explicitly include a discount factor, it induces a contraction mapping which allows temporal-difference approaches to converge to a fixed point. As $\lambda \rightarrow 1$, (6) also converges to the undiscounted objective (1). To show those, we first define the stochastic multi-step safety Bellman operator

$$T_{\lambda,\delta}[V](x_t) := \mathbb{E}_{n,s|x_t} \left[\max \{ \ell_t, \dots, \ell_{t+n-1}, b_t^{(n)} \} \right]. \quad (9)$$

We then present the theoretical results as follows. See Appendix A for proof.

Theorem 1 (Contraction Mapping). *The stochastic multi-step safety Bellman equation induces a contraction mapping under the supremum norm for $\lambda \in [0, 1)$ and $\delta \in [0, 1)$. Namely, for $V, \tilde{V} : \mathcal{X} \rightarrow \mathbb{R}$, there exists a constant $\rho \in [0, 1)$ such that $\|T_{\lambda,\delta}[V] - T_{\lambda,\delta}[\tilde{V}]\|_\infty \leq \rho \|V - \tilde{V}\|_\infty$.*

Proposition 1 (Value Approximation). *In the limit of $\lambda \rightarrow 1$, the fixed-point solution to (6) converges to the undiscounted safety value (1).*

Hence, (6) has a unique fixed-point (by Theorem 1) which solves the objective (1) as $\lambda \rightarrow 1$ (by Proposition 1). These properties justify the learning of V^π by regression towards

$$y_t^{(n)} := \max \{ \ell_t, \ell_{t+1}, \dots, \ell_{t+n-1}, b_t^{(n)} \} \quad (10)$$

which is a stochastic multi-step estimator that integrates safety signals observed along the trajectory segment while retaining the ability to bootstrap from the current value approximation at the stopping state. We refer to this learning procedure as λ -Reachability, in analogy to TD(λ) methods for cumulative rewards. Notably, the bootstrap horizon n above is unbounded, whereas in practice we only have access to finite-length policy rollouts. Hence, for practical implementation, we instead sample n from a truncated geometric distribution. See Appendix B for full training implementations.

3.2 Interpretations

Explicit Safety Horizon. The expected stopping length is $\mathbb{E}[n] = \frac{1}{1-\lambda}$ which increases monotonically as $\lambda \rightarrow 1$. λ provides an explicit mechanism for tuning the safety horizon: smaller values emphasize near-term safety, while larger values aggressively propagate long-horizon safety information. This control can be particularly useful when different notions of safety prediction are needed.

Relation to Discounted Safety Bellman. Two properties must hold to allow temporal-difference learning: (i) a unique fixed point induced by a contraction for training stability and (ii) consistency with the true safety value for value approximation accuracy. While both (3) and (6) satisfy these conditions, they differ fundamentally in how contraction is induced. The discounted Bellman induces contraction via explicit value discounts (3), requiring $\gamma < 1$. Meanwhile, accurate value approximation is achieved in the limit $\gamma \rightarrow 1$ [21]. Hence, the training stability and approximation accuracy are inherently coupled. In contrast, λ -Reachability (6) incorporates the bootstrapped value with probability δ^n , inducing a contraction mapping as long as $\delta < 1$. The value approximation accuracy is determined by a different parameter λ . Such decoupling allows one to improve value accuracy by annealing λ to 1, while maintaining contraction and training stability by $\delta < 1$.

Relation to CBF and HJ. For safety value learning, CBF-based approaches [16] directly exploit invariance labels that encode infinite-horizon safety, consistent with (1). These methods learn the persistent safety, but do not explicitly model how safety information propagates across timesteps. In contrast, HJ reachability approaches [1] rely on one-step self-consistency conditions (2) and propagate safety information through bootstrapping. While effective, purely local updates can be slow in high-dimensional settings. In this regard, λ -Reachability unifies these two paradigms via observing future safety signals with a stochastic look-ahead horizon, and interpolating between global invariance supervision and local HJ consistency. From (6), one can recover CBF learning by fixing $s = 0$ and using trajectory-specific horizons n , and recover HJ learning by fixing $s = 1$ and $n = 1$.

4 Experiments

4.1 Tasks

1) Policy training. Given a task, we first train a policy π using task-specific objectives (e.g., velocity tracking). Note that a safety value can be learned for an arbitrary policy.

2) Policy rollout. Given π , we collect a set of finite-length rollouts $\{\tau^\pi\}$ from the safety value learning environment. To collect unsafe scenarios, we sample a random event that perturbs the robot towards unsafe regions at the start of each episode. If the episode ends in a safe state, the robot is assumed to remain safe with a sufficiently trained policy. This enables us to label infinite-horizon safety metrics (i.e., signs and safety margins) from finite trajectories for evaluation. In practice, such an assumption may not hold, making safety labels empirical estimates that can be biased.

3) Safety labeling. For each state $x_t \in \tau^\pi$, we first compute the safety signal $\ell(x)$. Then, we define the forward-invariance indicator $c_t \triangleq \mathbf{1}\{\ell(x_k) \leq 0, \forall k \geq t\}$. Since rollouts are finite, c_t serves as the best available estimate of forward invariance, rather than the true infinite-horizon label. Second, we define the empirical safety value $\bar{V}^\pi(x_t) \triangleq \max_{k \geq t} \ell(x_k)$. The resulting dataset is $\mathcal{D} \triangleq \{(x_t, \ell_t, c_t, \bar{V}^\pi(x_t))\}_t$. Tasks used in this work are defined below. See Figure 2 for visualizations.

G1FLAT. We train a locomotion policy π for a Unitree G1 humanoid robot with 37 DoF in a flat environment with velocity-tracking goals. In this task, we consider a safety signal ℓ_{flat} to indicate the balance status, defined by both root height and body orientation.

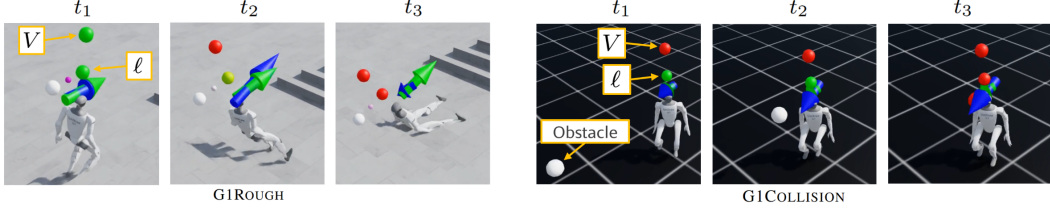


Figure 2: Humanoid safety value tasks. The safety signal ℓ is indicated by the ball color, with green indicating safe states ($\ell \leq -0.5$), yellow indicating near violations ($\ell \in (-0.5, 0]$), and red indicating safety violations ($\ell > 0$). The predicted safety value V is indicated by the higher ball with the same color coding.

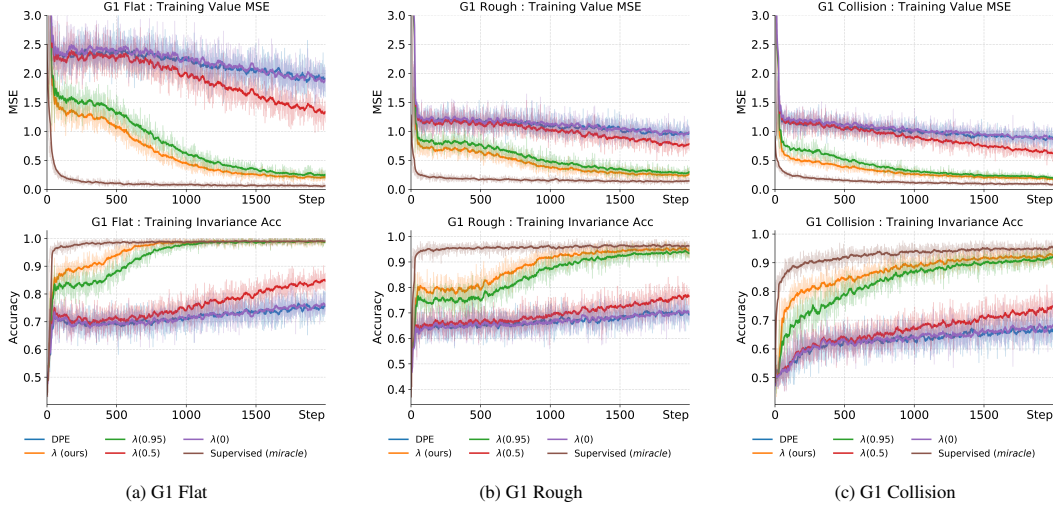


Figure 3: Training curves for safety value functions in different safety tasks. The top row shows the sample value error e_V during training, while the bottom row shows the invariant state classification accuracy.

G1ROUGH. This task replaces the flat ground in G1Flat with rough terrains with slopes and stairs with scan points as additional input. Other settings remain the same.

G1COLLISION. This task builds on G1FLAT and introduces dynamic obstacles that the robot must avoid while navigating. To calculate the safety signal $\ell_{\text{collision}}$, we introduce a distance component $\ell_{\text{dist}} = \min\{\max\{(d_{\min} - d)/d_{\min}, -1\}, 0\}$ and a contact component $\ell_{\text{contact}} = 1$ if the ball hits the robot and -1 otherwise. Hence, we have $\ell_{\text{collision}} = \max\{\ell_{\text{flat}}, \ell_{\text{dist}}, \ell_{\text{contact}}\}$.

See Appendix C for full environment setup, policy training, and data collection details.

4.2 Ablations and Baselines

λ -Reachability is trained by regressing towards the geometric-horizon targets (10) by minimizing

$$\mathcal{L}_{\text{main}} = \mathbb{E}_{x_t \sim \tau^\pi, n \sim \text{Geom}(1-\lambda)} \|V^\pi(x_t) - y_t^{(n)}\|^2 \quad (11)$$

via gradient descent with a learning rate of $\alpha = 1e - 3$ for 2000 steps. λ is set to 0.99. To examine the effect of λ value, we deploy ablations by setting alternative λ values in $\{0.95, 0.5, 0.0\}$. We also compare λ to other baselines that recover the safety value (1).

Discounted Policy Evaluation (DPE). DPE [21] recovers V^π by regressing towards the discounted safety Bellman target (3). The discount factor γ is initialized to 0.5 and annealed to 1.0 during training. This serves as the main baseline which λ -Reachability builds on.

Supervised (SV). SV fits the estimated safety value $\bar{V}^\pi(x_t)$. This represents the optimum in highly controlled tasks. In general, it is difficult to identify “events” and segment trajectories into finite episodes that capture infinite-horizon safety. Labels from partial trajectories would be biased. Hence, SV is considered a miracle baseline for evaluation only, rather than a practical method.

Table 1: Inference results (mean \pm std) in simulation. **Supervised** is marked as the miracle baseline. Best values among non-miracle methods are shown in bold.

Method	G1FLAT			G1ROUGH			G1COLLISION		
	r_{temp} (%)	e_V	r_{FPR} (%)	r_{temp} (%)	e_V	r_{FPR} (%)	r_{temp} (%)	e_V	r_{FPR} (%)
λ (ours)	99.98 \pm 0.21	0.09 \pm 0.19	0.21	97.92 \pm 9.24	0.08 \pm 0.22	6.49	99.40 \pm 4.79	0.13 \pm 0.23	6.12
λ (0.95)	99.97 \pm 0.29	0.11 \pm 0.23	0.38	96.43 \pm 11.34	0.09 \pm 0.25	9.23	98.63 \pm 5.96	0.12 \pm 0.20	9.15
λ (0.5)	56.52 \pm 20.39	0.71 \pm 1.23	31.91	52.40 \pm 27.65	0.27 \pm 0.64	45.45	44.80 \pm 18.28	0.16 \pm 0.33	48.02
λ (0.0)	26.39 \pm 14.09	1.00 \pm 1.65	47.42	21.97 \pm 19.06	0.39 \pm 0.88	60.17	23.85 \pm 14.53	0.18 \pm 0.38	59.63
DPE	22.05 \pm 12.30	1.04 \pm 1.70	49.31	21.94 \pm 16.66	0.40 \pm 0.89	59.68	22.61 \pm 14.50	0.18 \pm 0.37	60.47
Supervised	99.99 \pm 0.33	0.05 \pm 0.13	0.09	99.35 \pm 6.29	0.09 \pm 0.17	2.71	99.72 \pm 2.60	0.14 \pm 0.27	2.05

4.3 Metrics

For each state, the safety value function V^π should correctly reveal both (a) whether the system will stay safe and (b) the current safety margin. When applied as a safety monitor, V^π should alarm about future unsafe states as early as possible. That leads to the following metrics.

Temporal Recall r_{temp} is the ratio of the predictive horizon for unsafe states over the maximal possible horizon: $r_{\text{temp}} = \mathbb{E}_{\tau^\pi}[\max(0, t_{\text{unsafe}} - \hat{t}_{\text{unsafe}})/(t_{\text{unsafe}} - t_0)]$ where $t_{\text{unsafe}}, \hat{t}_{\text{unsafe}}$ are the earliest timestep when $\ell, V^\pi(x_t) \geq 0$. $r_{\text{temp}} = 1$ indicates the optimal value.

Sample Value Error e_V is the mean squared error $e_V = \mathbb{E}_{x_t \sim \tau^\pi} |V^\pi(x_t) - \bar{V}^\pi(x_t)|^2$.

Sample False Positive Rate r_{FPR} indicates the chances that V^π misclassifies a non-invariant state $r_{\text{FPR}} = p(V^\pi(x_t) \leq 0 \mid c_t = 0)$.

4.4 Quantitative Results in Simulation

We summarize the training results in Figure 3 and present evaluations in Table 1. See Appendix C for implementation details. Notably, G1FLAT is already a challenging safety value learning problem, with substantially higher state dimensionality than prior benchmarks [13, 1]. G1ROUGH further increases the complexity through height-map perception, while G1COLLISION is challenging in safety reasoning with multiple constraints.

Baselines. From Figure 3, we see that λ -Reachability quickly reduces the safety value prediction error and improves the invariance classification accuracy. The performance converges to that of the miracle baseline, showing that λ -Reachability is able to learn near-optimal safety value even with partial trajectories. On the other hand, discounted policy evaluation (DPE) has trouble in improving both metrics. Since DPE relies on fixed one-step updates (3), the propagation of unsafe events can be slow and cause inefficient learning in high-dimensional tasks. The above gap is also pronounced in Table 1 where λ -Reachability shows significant advantage over DPE in early warning of impending safety violations, accurate safety margins and rare false positives. With those, λ -Reachability validates as an efficient and reliable approach to high-dimensional safety value learning.

Ablations. From both Figure 3 and Table 1, we see that the choice of λ has a major impact on the performance. With $\lambda = 0.99$, λ -Reachability achieves near-optimal safety learning across all tasks, matching the performance of the miracle baseline. As λ decreases, the expected bootstrap horizon drops according to Section 3.2, e.g., 20 steps at $\lambda = 0.95$ and 2 steps at $\lambda = 0.5$. That quickly degrades the performance until it matches the performance of DPE at $\lambda = 0$. This agrees with the fact that with $\lambda = 0$, the horizon sampling (8) becomes deterministic and always samples 1, effectively reducing the target (10) to the one-step baseline (5) with $\gamma = 1$. Hence, we confirm that local bootstrapping cannot reliably propagate future safety violations, especially when safety-relevant events occur far from the current state.

4.5 Hardware Experiments

We perform G1FLAT and G1COLLISION tasks on a real Unitree G1 humanoid. V^π is learned in simulation and applied to physical rollout data. To perturb the safety signal, we push the robot

Table 2: Hardware inference results (mean \pm std) on real G1FLAT and G1COLLISION tasks.

Method	G1FLAT			G1COLLISION		
	r_{temp} (%)	e_V	r_{FPR} (%)	r_{temp} (%)	e_V	r_{FPR} (%)
λ (ours)	80.91 \pm 4.96	0.19 \pm 0.15	20.31	73.59 \pm 9.20	0.48 \pm 0.25	30.54
λ (0.95)	82.24 \pm 10.15	0.21 \pm 0.16	20.31	72.09 \pm 9.13	0.47 \pm 0.25	31.83
λ (0.5)	84.26 \pm 11.78	0.24 \pm 0.14	18.77	48.78 \pm 27.09	0.58 \pm 0.33	48.35
λ (0.0)	74.25 \pm 22.35	0.26 \pm 0.19	31.80	41.29 \pm 23.66	0.66 \pm 0.39	53.99
DPE	62.07 \pm 19.42	0.44 \pm 0.32	45.21	13.52 \pm 6.97	0.75 \pm 0.52	72.20
Supervised	84.42 \pm 13.26	0.27 \pm 0.26	19.92	79.63 \pm 9.67	0.48 \pm 0.33	23.21

in G1FLAT and throw balls at the robot in G1COLLISION where the robot and ball are tracked using a mocap system. We summarize results in Table 2. λ -Reachability stably outperforms the DPE baseline, and matches the performance of the miracle baseline with proper hyperparameters. Results on the G1COLLISION task show trends similar to those in the previous section. For G1FLAT, however, λ -Reachability with high λ values shows less advantage, with top scores at $\lambda = 0.5$. One potential cause is that V^π in G1FLAT relies entirely on noisy, real proprioceptive signals. λ trained in simulation with longer bootstrap horizons (i.e., larger λ) relies on predictable future trajectories, which are rare in practice. λ with shorter horizons leans more on the near-term signal and is more robust under distribution shift. In G1COLLISION, although the same noises exist, the safety values largely depend on the obstacle, whose trajectories are smooth and predictable thanks to the mocap system. See Appendix C for training details and Appendix D for additional results.

5 Limitations

We identify two aspects where future work would benefit. First, safety value learning requires infinite-horizon trajectories to be sampled, since the horizon is essentially unbounded (see (8)). In practice, however, policy rollouts are finite with truncated horizon sampling (see (13)). Hence, practical λ learning can be biased. It is thus beneficial to derive a max-horizon-dependent term as future work to quantify the learning bias with truncated bootstrap horizons. Another aspect regards the tradeoff between bias and robustness. As shown previously, noisy real data can introduce distributional shifts that degrade the performance of long-horizon λ values. On the other hand, the solution to (6) is unbiased only when λ anneals to 1. Consequently, λ values closer to 1 reduce bias while making the learned value less robust against noisy online input. A principled approach to the bias-robustness tradeoff would be beneficial for applying λ in general conditions.

6 Discussions and Conclusions

In this paper, we proposed λ -Reachability, a safety value learning approach that solves the safety Bellman equation using a geometric mixture of multi-step max backups. λ -Reachability induces both a contraction mapping and unbiased safety value approximation under mild conditions, enabling scalable and efficient temporal-difference learning approaches. Experiments across multiple value learning problems demonstrate that λ -Reachability consistently outperforms the baseline, addressing the issue of slow information propagation inherent to one-step bootstrapping in high-dimensional settings. Although this work focuses on policy evaluation and does not derive a control policy, it can be directly integrated into existing reinforcement learning frameworks to enable safety-aware learning. For instance, λ -Reachability can replace value learning in actor-critic methods (e.g., TD3, SAC), yielding actor updates that explicitly maximize safety. This improves upon prior actor-critic-based safety approaches such as [9], in which value functions need only be correct up to a partial order. Crucially, safety-maximizing actor-critics rely on accurate value scales to determine the feasibility of actions and will therefore benefit from the accurate safety margins of λ . Similarly, λ can be used in policy optimization (e.g., TRPO, PPO) by replacing value targets with geometric-horizon max targets (10), similar to [21]. Hence, while λ -Reachability focuses on policy evaluation, it provides a principled approach to learning high-dimensional safety values, which is beneficial across a broad class of safe policy learning problems.

References

- [1] M. Ganai, S. Gao, and S. L. Herbert. Hamilton-jacobi reachability in reinforcement learning: A survey. *IEEE Open Journal of Control Systems*, 3:310–324, 2024.
- [2] C. Liu and M. Tomizuka. Control in a safe set: Addressing safety in human-robot interactions. In *Dynamic Systems and Control Conference*, volume 46209. American Society of Mechanical Engineers, 2014.
- [3] R. Liu, R. Chen, and C. Liu. Safe interactive industrial robots using jerk-based safe set algorithm. *arXiv preprint arXiv:2204.03038*, 2022.
- [4] A. D. Ames, S. Coogan, M. Egerstedt, G. Notomista, K. Sreenath, and P. Tabuada. Control barrier functions: Theory and applications. In *2019 18th European Control Conference (ECC)*, 2019. doi:10.23919/ECC.2019.8796030.
- [5] H. Wang, J. Peng, J. Xu, F. Zhang, and Y. Wang. High-order control barrier functions-based optimization control for time-varying nonlinear systems with full-state constraints: A dynamic sub-safe set approach. *International Journal of Robust and Nonlinear Control*, 33(8):4490–4503, 2023.
- [6] J. F. Fisac, A. K. Akametalu, M. N. Zeilinger, S. Kaynama, J. Gillula, and C. J. Tomlin. A general safety framework for learning-based control in uncertain robotic systems. *IEEE Transactions on Automatic Control*, 64(7):2737–2752, 2019. doi:10.1109/TAC.2018.2876389.
- [7] K.-C. Hsu, A. Z. Ren, D. P. Nguyen, A. Majumdar, and J. F. Fisac. Sim-to-lab-to-real: Safe reinforcement learning with shielding and generalization guarantees. *Artificial Intelligence*, 314:103811, 2023.
- [8] K. S. Yun, R. Chen, C. Dunaway, J. M. Dolan, and C. Liu. Safe control of quadruped in varying dynamics via safety index adaptation. *arXiv preprint arXiv:2409.09882*, 2024.
- [9] R. Pandya, C. Liu, and A. V. Bajcsy. Robots that learn to safely influence via prediction-informed reach-avoid dynamic games. In *2025 IEEE International Conference on Robotics and Automation (ICRA)*, 2025. doi:10.1109/ICRA55743.2025.11128803. URL <https://arxiv.org/abs/2409.12153>. arXiv:2409.12153.
- [10] K. Leung, E. Schmerling, M. Zhang, M. Chen, J. Talbot, J. C. Gerdes, and M. Pavone. On infusing reachability-based safety assurance within planning frameworks for human-robot vehicle interactions. *The International Journal of Robotics Research*, 39(10-11):1326–1345, 2020.
- [11] T. He, C. Zhang, W. Xiao, G. He, C. Liu, and G. Shi. Agile but safe: Learning collision-free high-speed legged locomotion. *arXiv preprint arXiv:2401.17583*, 2024.
- [12] R. Chen, W. Zhao, R. Liu, W. Zhang, and C. Liu. Real-time safety index adaptation for parameter-varying systems via determinant gradient ascend. *arXiv preprint*, 2023.
- [13] R. Chen, W. Zhao, and C. Liu. Safety index synthesis with state-dependent control space. *arXiv preprint*, 2023.
- [14] W. Zhao, T. He, T. Wei, S. Liu, and C. Liu. Safety index synthesis via sum-of-squares programming, 2022. URL <https://arxiv.org/abs/2209.09134>. Also appears in ACC 2023 (doi:10.23919/ACC55779.2023.10156463).
- [15] A. A. Ahmadi and A. Majumdar. Dsos and sdsos optimization: more tractable alternatives to sum of squares and semidefinite optimization. *SIAM Journal on Applied Algebra and Geometry*, 3(2):193–230, 2019.

- [16] L. Lindemann, A. Robey, D. V. Dimarogonas, S. Tu, N. Matni, and R. Tedrake. Learning hybrid control barrier functions from data. In *Proceedings of the 4th Conference on Robot Learning*, volume 155 of *Proceedings of Machine Learning Research*, 2021. URL <https://proceedings.mlr.press/v155/lindemann21a.html>.
- [17] T. Vertovec and A. Clark. Scalable verification of neural control barrier functions using linear bound propagation. *arXiv preprint*, 2025.
- [18] H. Zhang, Z. Qin, S. Gao, and A. Clark. Seev: Efficient and sound neural network verification for safety-critical barrier certificates, 2024. URL <https://arxiv.org/abs/2410.20326>.
- [19] S. Bansal, M. Chen, S. Herbert, and C. J. Tomlin. Hamilton-jacobi reachability: A brief overview and recent advances. In *2017 IEEE 56th Annual Conference on Decision and Control (CDC)*, 2017. doi:10.1109/CDC.2017.8263977. arXiv:1709.07523.
- [20] J. Darbon and S. Osher. Algorithms for overcoming the curse of dimensionality for certain hamilton–jacobi equations arising in control theory and elsewhere, 2016. URL <https://arxiv.org/abs/1605.01799>.
- [21] J. F. Fisac, N. F. Lugovoy, V. Rubies-Royo, S. Ghosh, and C. J. Tomlin. Bridging hamilton-jacobi safety analysis and reinforcement learning. In *2019 International Conference on Robotics and Automation (ICRA)*, pages 8550–8556. IEEE, 2019.
- [22] K.-C. Hsu, V. Rubies-Royo, C. J. Tomlin, and J. F. Fisac. Safety and liveness guarantees through reach-avoid reinforcement learning. In *Proceedings of Robotics: Science and Systems*, 2021. doi:10.15607/RSS.2021.XVII.077. URL <https://www.roboticsproceedings.org/rss17/p077.pdf>.
- [23] M. Ganai, Z. Gong, C. Yu, S. Herbert, and S. Gao. Iterative reachability estimation for safe reinforcement learning. In *Advances in Neural Information Processing Systems*, 2023. URL https://papers.nips.cc/paper_files/paper/2023/file/dca63f2650fe9e88956c1b68440b8ee9-Paper-Conference.pdf.
- [24] R. S. Sutton. Learning to predict by the methods of temporal differences. *Machine Learning*, 3(1):9–44, 1988. doi:10.1023/A:1022633531479.
- [25] W. Zhao, T. He, T. Wei, S. Liu, and C. Liu. Safety index synthesis via sum-of-squares programming. In *ACC*, pages 732–737. IEEE, 2023.
- [26] S. Fujimoto, H. Hoof, and D. Meger. Addressing function approximation error in actor-critic methods. In *International conference on machine learning*, pages 1587–1596. PMLR, 2018.

A Proof of Contraction Mapping

Theorem 2 (Contraction Mapping). *The stochastic multi-step safety Bellman equation induces a contraction mapping under the supremum norm for $\lambda \in [0, 1)$ and $\delta \in [0, 1)$. Namely, for $V, \tilde{V} : \mathcal{X} \rightarrow \mathbb{R}$, there exists a constant $\rho \in [0, 1)$ such that $\|T_{\lambda, \delta}[V] - T_{\lambda, \delta}[\tilde{V}]\|_\infty \leq \rho \|V - \tilde{V}\|_\infty$.*

Proof. For brevity, let $m_t^{(n)} := \max_{t \leq k \leq t+n-1} \ell_k$. Let $V_t \equiv V(x_t)$ and expand the terminal sampling, we have

$$\begin{aligned} T_{\lambda, \delta}[V](x_t) &= \mathbb{E}_{n|x_t} \left[\delta^n \max(m_t^{(n)}, V_{t+n}) \right. \\ &\quad \left. + (1 - \delta^n) \max(m_t^{(n)}, v_{\text{term}}) \right]. \end{aligned} \quad (12)$$

Then, $\forall x_t \in \mathcal{X}$,

$$\begin{aligned} & \left| T_{\lambda, \delta}[V](x_t) - T_{\lambda, \delta}[\tilde{V}](x_t) \right| \\ &= \left| \mathbb{E}_{n|x_t} \left[\delta^n (\max(m_t^{(n)}, V_{t+n}) - \max(m_t^{(n)}, \tilde{V}_{t+n})) \right] \right| \\ &\leq \mathbb{E}_{n|x_t} \left[\delta^n \left| \max(m_t^{(n)}, V_{t+n}) - \max(m_t^{(n)}, \tilde{V}_{t+n}) \right| \right] \\ &\leq \mathbb{E}_{n|x_t} \left[\delta^n \left| V_{t+n} - \tilde{V}_{t+n} \right| \right] \\ &\leq \mathbb{E}_{n|x_t} [\delta^n] \sup_x \left| V(x) - \tilde{V}(x) \right| \\ &= \mathbb{E}_{n|x_t} [\delta^n] \|V - \tilde{V}\|_\infty. \end{aligned}$$

Hence, we have $\|T_{\lambda, \delta}[V] - T_{\lambda, \delta}[\tilde{V}]\|_\infty \leq \mathbb{E}_{n|x_t} [\delta^n] \|V - \tilde{V}\|_\infty$. The contraction factor is indeed $\rho = \mathbb{E}_{n|x_t} [\delta^n] \in [0, 1)$. \square

B λ -Reachability Implementation

B.1 Practical Implementations

Truncated Geometric Distribution. In practice, trajectories are finite and only a limited number of future states are available for each anchor time step. Sampling from an untruncated geometric distribution would therefore place non-negligible probability mass on horizons beyond the available data, implicitly biasing updates toward terminal states. To address this issue, we sample the bootstrap horizon from a truncated geometric distribution with finite support and renormalized probabilities,

$$\mathbb{P}(n = k) = \frac{(1 - \lambda)\lambda^{k-1}}{1 - \lambda^{T-t}}, \quad k \in \{1, \dots, T - t\}, \quad (13)$$

where T denotes the terminal time of the trajectory. This truncation preserves the geometric structure of the stopping distribution while ensuring that all sampled horizons are feasible given the available data.

Value Initialization. Safety signals $\ell(x)$ are non-positive within the safe set, and the reachability update relies on a max operator over future safety values. As a consequence, initializing the value function with overly pessimistic (positive) values can lead to self-reinforcing errors, whereby spurious unsafe predictions are repeatedly propagated backward through bootstrapping. To prevent this failure mode, we initialize the value function conservatively as

$$V_0^\pi(x) \leq \min_x \ell(x), \quad (14)$$

which guarantees that early bootstrapped targets are dominated by observed safety signals rather than inaccurate value estimates. This initialization bias is gradually corrected as unsafe events are encountered during training. In practice, we assign $V_0^\pi(x)$ to a constant which is by design a lower bound of ℓ .

Stabilizing Training. We adopt several stabilization techniques from value-based learning to improve robustness under bootstrapped max backups. First, we use a slowly-updated target network to compute bootstrap values in (10). Concretely, we maintain two online critics $V_{\theta_1}^\pi, V_{\theta_2}^\pi$ and their corresponding target networks $V_{\bar{\theta}_1}^-, V_{\bar{\theta}_2}^-$. Following the clipped target idea in double-Q methods [26], we compute the bootstrap term conservatively as

$$V_{\text{boot}}^-(x) := \min\{V_{\bar{\theta}_1}^-(x), V_{\bar{\theta}_2}^-(x)\}, \quad (15)$$

and use $V_{\text{boot}}^-(x_{t+n})$ in place of $V_\pi(x_{t+n})$ in (10). Both online critics regress to the same target, which substantially reduces the propagation of spurious over-estimation through the max operator. Target networks are updated via Polyak averaging, $\bar{\theta} \leftarrow (1 - \tau)\bar{\theta} + \tau\theta$.

B.2 λ -Reachability Training Procedures

Algorithm 1 λ -Reachability Training

Require: Dataset of trajectories $\{\tau\}$ collected under policy π

Require: Geometric parameter $\lambda \in (0, 1)$; terminal condition parameter $\delta \in (0, 1)$; absorption safety value $v_{\text{term}} \leq \min_x \ell(x)$; batch size B ; max horizon n_{max} ; learning rate α ; Polyak rate τ

- 1: **Initialize** two online critics $V_{\theta_1}^\pi, V_{\theta_2}^\pi$ conservatively (e.g., $V_{\theta_j}^\pi(x) \leq \min_x \ell(x)$)
- 2: **Initialize** target critics $V_{\bar{\theta}_1}^- \leftarrow V_{\theta_1}^\pi, V_{\bar{\theta}_2}^- \leftarrow V_{\theta_2}^\pi$
- 3: **for** each training iteration **do**
- 4: Sample a minibatch of anchor indices $\{(\tau_i, t_i)\}_{i=1}^B$ with futures available up to n_{max}
- 5: **for** each sample $i = 1, \dots, B$ **do**
- 6: Let $x_i \leftarrow x_{t_i}^{\tau_i}, x_i^+ \leftarrow x_{t_i+1}^{\tau_i}$, and $\ell_i \leftarrow \ell(x_i)$
- 7: Let $\bar{n}_i \leftarrow \min(T_i - t_i, n_{\text{max}})$
- 8: Sample horizon $n_i \sim \text{TruncGeom}(1 - \lambda; 1, \bar{n}_i)$, i.e.,

$$\mathbb{P}(n_i = k) = \frac{(1 - \lambda)\lambda^{k-1}}{1 - \lambda^{\bar{n}_i}}, \quad k \in \{1, \dots, \bar{n}_i\}$$

- 9: Compute conservative bootstrap

$$V_i \leftarrow \min\left\{V_{\bar{\theta}_1}^-(x_{t_i+n_i}^{\tau_i}), V_{\bar{\theta}_2}^-(x_{t_i+n_i}^{\tau_i})\right\}$$

- 10: Sample terminal condition

$$s_i \sim \text{Bernoulli}(\delta^{n_i})$$

- 11: Compute max target

$$y_i \leftarrow \max\{\ell(x_{t_i}^{\tau_i}), \dots, \ell(x_{t_i+n_i-1}^{\tau_i}), s_i V_i + (1 - s_i)v_{\text{term}}\}$$

- 12: Evaluate online critics:

$$v_{j,i} \leftarrow V_{\theta_j}^\pi(x_i), \quad j \in \{1, 2\}$$

- 13: Compute loss (mean over batch):

$$\mathcal{L} \leftarrow \frac{1}{B} \sum_{i=1}^B \sum_{j=1}^2 (v_{j,i} - y_i)^2$$

- 14: Gradient step:

$$\theta_j \leftarrow \theta_j - \alpha \nabla_{\theta_j} \mathcal{L}, \quad j \in \{1, 2\}$$

- 15: Update target critics (Polyak averaging):

$$\bar{\theta}_j \leftarrow (1 - \tau)\bar{\theta}_j + \tau\theta_j, \quad j \in \{1, 2\}$$

C Implementation Details

We present the implementation details of the entire pipeline used to train and evaluate safety value functions for the G1FLAT, G1ROUGH, and G1COLLISION tasks both in simulation and on physical hardware. For each task, we keep the humanoid modeling consistent across policy training, rollout collection, safety value learning, and safety value inference. For simulation inference, all stages are performed in simulation. For hardware inference, all stages except the safety value inference are done in simulation. Adaptations are made to accommodate the absence of certain hardware observations, for example, link-obstacle contact signals.

All training and inference steps are performed on a single workstation equipped with an NVIDIA RTX 4090 (24 GB) GPU, running PyTorch 2.7.0+cu128, Python 3.11, IsaacLab 0.46, and `rsl_rl`.

C.1 Robot Policy Training

We first describe the environment setup and training details for acquiring the robot policy π .

C.1.1 Policy Training for Safety Value Inference in Simulation

For simulation experiments in Section 4.4, we use a Unitree G1 humanoid robot with 34 DoF. The observation spaces for all three tasks are listed in Table 3.

Table 3: Observation composition for the simulation policies. All entries are single-frame dimensions (no history stacking). The critic shares the actor’s observation group (symmetric actor–critic).

Observation segment	G1FLAT	G1ROUGH	G1COLLISION
Base linear velocity $\mathbf{v} \in \mathbb{R}^3$	3	3	3
Base angular velocity $\boldsymbol{\omega} \in \mathbb{R}^3$	3	3	3
Projected gravity $\mathbf{g} \in \mathbb{R}^3$	3	3	3
Velocity command $\mathbf{c} \in \mathbb{R}^3$	3	3	3
Joint positions $\mathbf{q} \in \mathbb{R}^{37}$	37	37	37
Joint velocities $\dot{\mathbf{q}} \in \mathbb{R}^{37}$	37	37	37
Last action $\mathbf{a} \in \mathbb{R}^{37}$	37	37	37
Height scan $\mathbf{s}_{\text{scan}} \in \mathbb{R}^{187}$ (17×11 grid, 0.1 m)	—	187	—
Ball position in base frame $\mathbf{p}_{\text{ball}} \in \mathbb{R}^3$	—	—	3
Ball velocity in base frame $\mathbf{v}_{\text{ball}} \in \mathbb{R}^3$	—	—	3
Total observation dimension	123	310	129

In G1FLAT and G1ROUGH, the safety signal is defined as

$$\ell_{\text{flat}} := \max \{ \ell_{\text{root}}, \ell_{\text{ori}} \}, \text{ where } \ell_{\text{root}} = -\frac{h_{\text{root}} - h_{\text{min}}}{h_{\text{root}}^* - h_{\text{min}}}, \ell_{\text{ori}} = \frac{\psi_g - \psi_{\text{max}}}{\psi_{\text{max}}}. \quad (16)$$

The robot is considered to be safe and balanced if (a) its root height h_{root} is higher than the threshold $h_{\text{min}} = 0.2m$ and (b) the deviation ψ_g between the root Z axis and gravity is at most $\psi_{\text{max}} = \pi/4$. $h_{\text{root}}^* = 0.65m$ is the default standing root height.

In G1COLLISION, a lightweight ball (50g, 10cm radius) is spawned every 3 to 5 seconds and launched toward the humanoid robot. The ball spawns at a random position at $[2m, 5m]$ from the robot, at heights between $[0.1m, 1.2m]$, and is given an initial velocity of $[3m/s, 6m/s]$ aimed at the robot’s torso at 0.8m height with gravity compensation to follow a ballistic arc.

Rewards used for training π are summarized in Table 4.

The policy π for all tasks is an MLP with feed-forward layers with ELU activations and a Gaussian action head (initial scalar standard deviation 1.0, no observation normalization). The hidden sizes are $[256, 128, 128]$ for G1FLAT and G1COLLISION and $[512, 256, 128]$ for G1ROUGH; the output dimension matches the action space (37), and joint-position targets are recovered as $\mathbf{q}^{\text{target}} = \mathbf{q}^{\text{def}} + 0.5 \mathbf{a}$ (scale 0.5, default-offset on, no action clipping). The policy is trained with PPO for 1000 steps with 2048 parallel agents in IsaacLab. Hyperparameter used are listed in Table 5.

Table 4: Reward composition for the simulation PPO policies. A dash (—) means the term is not used for that task. For G1COLLISION the ball-related terms are curriculum-gated, becoming active only after iteration 500; episodes terminate at 20 s or on illegal torso_link contact (>1 N), with ball impacts above 0.4 m excluded from termination.

Term	Formula	G1FLAT	G1ROUGH	G1COLLISION
Lin. vel. tracking	$\exp(-\ \mathbf{v}_{xy} - \mathbf{c}_{xy}\ ^2/\sigma^2)$ $\sigma=0.5$	1.0	1.0	1.0
Ang. vel. tracking	$\exp(-(\omega_z - c_{\omega_z})^2/\sigma^2)$ $\sigma=0.5$	1.0	2.0	1.0
z -velocity penalty	v_z^2	-0.2	0	-0.2
Roll/pitch penalty	$\ \boldsymbol{\omega}_{xy}\ ^2$	-0.05	—	-0.05
Joint torques	$\ \boldsymbol{\tau}\ ^2$	-2×10^{-6}	-1.5×10^{-7}	-2×10^{-6}
Joint accelerations	$\ \ddot{\mathbf{q}}\ ^2$	-1×10^{-7}	-1.25×10^{-7}	-1×10^{-7}
Action rate	$\ \mathbf{a}_t - \mathbf{a}_{t-1}\ ^2$	-0.005	-0.005	-0.005
Feet air-time bonus	$\sum_f (t_f^{\text{air}} - \bar{t}) \mathbf{1}[\text{first contact}]$ $\bar{t}=0.4$ s	0.75	0.25	0.75
Feet slide	$\sum_f \ \mathbf{v}_f\ \mathbf{1}[\text{contact}]$	-0.1	-0.1	-0.1
Flat orientation	$\ \mathbf{g}_{xy}\ ^2$	-1.0	-1.0	-1.0
Joint-position limits	$\sum_j \max(0, q_j - q_j^{\text{max}})$ $+ \max(0, q_j^{\text{min}} - q_j)$	-1.0	-1.0	-1.0
Undesired contacts	$\sum_b \mathbf{1}[\ \mathbf{f}_b\ > 1 \text{ N}]$ (torso/arms)	-1.0	—	-1.0
Termination	$\mathbf{1}[\text{episode terminates}]$	-200	-200	-200
Joint deviation (hip)	$\sum_{j \in \text{hip}} (q_j - q_j^{\text{def}})^2$	—	-0.1	—
Joint deviation (arms)	$\sum_{j \in \text{arms}} (q_j - q_j^{\text{def}})^2$	—	-0.1	—
Joint deviation (fingers)	$\sum_{j \in \text{fingers}} (q_j - q_j^{\text{def}})^2$	—	-0.05	—
Joint deviation (torso)	$(q_{\text{torso}} - q_{\text{torso}}^{\text{def}})^2$	—	-0.1	—
Ball proximity	$\exp(-d_{\text{ball}}^2/\sigma^2)$, $\sigma=2.0$ m	—	—	-5.0
Ball collision	$\mathbf{1}[\ \mathbf{f}_{\text{ball}}\ > 0.1 \text{ N}]$	—	—	-1.0

Table 5: PPO hyperparameters for the simulation policies. All three tasks use the same algorithmic settings; only the network width and the number of training iterations vary per task. For all simulation tasks the actor and the critic consume the *same* observation group (symmetric actor-critic).

Optimiser	Adam, lr 1×10^{-3} , adaptive schedule (target KL 0.01)
Discount γ , GAE λ_{GAE}	0.99, 0.95
PPO clip / value-loss coef / entropy coef	0.2 / 1.0 / 0.008
Epochs per update / minibatches per update	5 / 4
Steps per environment per rollout	24
Parallel environments	4096
Max gradient norm	1.0
Iterations (G1FLAT / G1ROUGH / G1COLLISION)	1500 / 3000 / 1500
Random seed	42
Actor / critic observations	symmetric (no privileged terms)

C.1.2 Policy Training for Safety Value Inference in the Real World

For hardware experiments in Section 4.5, we use a Unitree G1 humanoid robot with 29 DoF to be consistent with the physical platform we have access to. The environment setup for G1FLAT and G1COLLISION is shown below.

Observation space. For deployment the observation history is stacked over the last 5 control steps (history length 5, control rate 50 Hz). Table 6 lists the per-frame composition and the resulting actor/critic dimensions. The actor uses only sensors that are also available on the physical platform (no base linear velocity), while the critic additionally observes $\mathbf{v} \in \mathbb{R}^3$ per frame: an *asymmetric* actor-critic.

Table 6: Observation composition for the 29-DoF hardware policies. The critic additionally consumes the base linear velocity \mathbf{v} per frame (privileged) and is therefore 3 dimensions per frame larger than the actor.

Observation segment (per frame)	G1FLAT	G1COLLISION
Base angular velocity $\boldsymbol{\omega} \in \mathbb{R}^3$	3	3
Projected gravity $\mathbf{g} \in \mathbb{R}^3$	3	3
Velocity command $\mathbf{c} \in \mathbb{R}^3$	3	3
Joint positions $\mathbf{q} \in \mathbb{R}^{29}$	29	29
Joint velocities $\dot{\mathbf{q}} \in \mathbb{R}^{29}$	29	29
Last action $\mathbf{a} \in \mathbb{R}^{29}$	29	29
Ball position in base frame $\mathbf{p}_{\text{ball}} \in \mathbb{R}^3$	—	3
Ball velocity in base frame $\mathbf{v}_{\text{ball}} \in \mathbb{R}^3$	—	3
Per-frame dimension	96	102
Actor observation (5-frame stack)	480	510
Critic observation (actor + \mathbf{v} /frame)	495	525

Rewards. Table 7 lists the reward terms used for training the two hardware policies. G1COLLISION (HW) is warm-started from the deployed G1FLAT (HW) baseline; the only additions in the avoidance policy are the three ball-related terms.

Table 7: Reward composition for the 29-DoF hardware policies. A dash (—) denotes a term not used for that task. Termination conditions: time-out (20 s), base height < 0.2 m, or projected-gravity tilt > 0.8 rad.

Term	Formula	G1FLAT (HW)	G1COLLISION (HW)
Lin. vel. tracking	$\exp(-\ \mathbf{v}_{xy} - \mathbf{c}_{xy}\ ^2/\sigma^2)$ $\sigma=0.5$	1.0	1.0
Ang. vel. tracking	$\exp(-(\omega_z - c_{\omega_z})^2/\sigma^2)$ $\sigma=0.5$	0.5	0.5
Alive bonus	1 per step	0.15	0.15
Flat orientation	$\ \mathbf{g}_{xy}\ ^2$	-5.0	-5.0
Joint-position limits	$\sum_j \max(0, q_j - q_j^{\max})$ $+ \max(0, q_j^{\min} - q_j)$	-5.0	-5.0
Undesired contacts	$\sum_b \mathbf{1}[\ \mathbf{f}_b\ > 1 \text{ N}]$ (excl. ankles)	-1.0	-1.0
Feet slide	$\sum_f \ \mathbf{v}_f\ \mathbf{1}[\text{contact}]$	-0.2	-0.2
Joint deviation (arms)	$\sum_{j \in \text{arms}} (q_j - q_j^{\text{def}})^2$	-0.1	-0.1
Joint deviation (waist)	$\sum_{j \in \text{waist}} (q_j - q_j^{\text{def}})^2$	-1.0	-1.0
Joint deviation (hip yaw/roll)	$\sum_{j \in \text{hip}} (q_j - q_j^{\text{def}})^2$	-1.0	-1.0
z -velocity penalty	v_z^2	-2.0	-2.0
Roll/pitch penalty	$\ \boldsymbol{\omega}_{xy}\ ^2$	-0.05	-0.05
Joint velocity	$\ \dot{\mathbf{q}}\ ^2$	-10^{-3}	-10^{-3}
Joint acceleration	$\ \ddot{\mathbf{q}}\ ^2$	-2.5×10^{-7}	-2.5×10^{-7}
Action rate	$\ \mathbf{a}_t - \mathbf{a}_{t-1}\ ^2$	-0.05	-0.05
Energy (Unitree)	$\sum_j \tau_j \dot{q}_j$	-2×10^{-5}	-2×10^{-5}
Base height	$(h_{\text{base}} - 0.78)^2$	-10.0	-10.0
Feet gait (Unitree)	period 0.8 s, offset $[0, 0.5]$, threshold 0.55	0.5	0.5
Feet clearance (swing)	$\sum_f (h_f - 0.1)^2 \mathbf{1}[\text{swing}]$	1.0	1.0
Ball proximity	$\exp(-d_{\text{ball}}^2/\sigma^2)$, $\sigma=2.0$ m	—	-5.0
Ball collision	$\mathbf{1}[\ \mathbf{f}_{\text{ball}}\ > 0.1 \text{ N}]$	—	-20.0
Ball approaching	$\max(0, -\dot{d}_{\text{ball}}) \cdot \mathbf{1}[d_{\text{ball}} \leq 2 \text{ m}]$	—	-2.0

PPO hyperparameters. Table 8 lists the PPO settings for the hardware policies. Both tasks use a [512, 256, 128] MLP with ELU activations and a Gaussian action head (init scalar std 1.0). Compared to the simulation lineage, the hardware policies use (i) wider networks, (ii) an asymmetric actor-critic, (iii) a smaller action scale ($\mathbf{q}^{\text{target}} = \mathbf{q}^{\text{def}} + 0.25 \mathbf{a}$, vs. 0.5 in simulation), and (iv)

a richer domain randomisation regime (friction sampling, base-mass perturbation, and a periodic root-velocity push event) to bridge to hardware.

Table 8: PPO hyperparameters for the 29-DoF hardware policies.

Hyperparameter	Value
Actor/critic hidden dimensions	[512, 256, 128]
Activation; action head	ELU; Gaussian, init scalar std 1.0
Observation normalisation	off (empirical normalisation on)
Optimiser	Adam, lr 10^{-3} , adaptive schedule (target KL 0.01)
Discount γ , advantage λ_{GAE}	0.99, 0.95
PPO clip / value-loss coef / entropy coef	0.2 / 1.0 / 0.01
Epochs per update / minibatches per update	5 / 4
Steps per environment per rollout	24
Parallel envs (G1FLAT / G1COLLISION)	8192 / 4096
Iterations (G1FLAT)	30 000 (deployed @ 6 000)
Iterations (G1COLLISION)	5 000 (deployed @ 4 999)
Warm start (G1COLLISION)	resume from deployed G1FLAT baseline
Observation history length	5 frames
Actor / critic observations	asymmetric ; critic adds $\mathbf{v} \in \mathbb{R}^3$ per frame friction $\in [0.3, 1.0]$; base mass $+[-1, 3]$ kg;
Domain randomisation	push every 5 s, $v_{x,y} \sim \mathcal{U}[-0.5, 0.5]$ m/s
Random seed	42

Sim-vs-hardware differences in PPO. The hardware lineage diverges from the simulation lineage in four respects. (i) *Asymmetric actor-critic.* Because the base linear velocity \mathbf{v} is not reliably observable on the deployed platform, it is withheld from the actor and provided only to the critic; the actor consumes 96 (G1FLAT) or 102 (G1COLLISION) dimensions per frame while the critic consumes 99 and 105, respectively. (ii) *Observation history.* Hardware observations are stacked over the last 5 frames (simulation uses single-frame observations). (iii) *Action scale.* Joint-position targets are recovered as $\mathbf{q}^{\text{target}} = \mathbf{q}^{\text{def}} + 0.25 \mathbf{a}$ on hardware versus $0.5 \mathbf{a}$ in simulation, halving the action range to reduce abrupt commands. (iv) *Domain randomisation.* Friction is sampled in $[0.3, 1.0]$, the torso mass is perturbed by $[-1, 3]$ kg, and a periodic root-velocity push event with $v_{x,y} \sim \mathcal{U}[-0.5, 0.5]$ m/s is applied every 5 s; the simulation lineage uses no such randomisation. All other PPO settings (optimiser, γ , λ_{GAE} , clip, value-loss/entropy coefficients, epochs and minibatches) are identical to the simulation policies.

C.2 Data Collection for Safety Value Learning

With robot policy π , the dataset \mathcal{D} for safety value learning is generated by evaluating π in each simulation environment with 2048 agents for 1000 steps. For simulation inference tasks in Section 4.4, safety signals are labeled following Section 4.1. For hardware inference in Section 4.5, we label the safety signal for G1FLAT as $\ell_{\text{flat}} := \ell_{\text{ori}}$. The contact component ℓ_{contact} in the safety signal for G1COLLISION is synthesized as $\ell_{\text{contact}} := 1_{d_{\text{ball}} \leq 0.3} - 1_{d_{\text{ball}} > 0.3}$.

C.3 Safety Value Learning

Using the dataset \mathcal{D} , we train the λ -Reachability approach, its ablations, and baselines. All safety values are represented as neural networks with two hidden layers of width 256 and ReLU activations, mapping each task’s observation to a scalar value $V^\pi(x) \in \mathbb{R}$. The final linear layer is initialised with zero weights and bias -2 , so that V^π starts strongly safe everywhere. For λ -Reachability

we instantiate two critics $V_{\theta_1}^\pi, V_{\theta_2}^\pi$ with this architecture and report the ensemble mean $V^\pi(x) = \frac{1}{2}(V_{\theta_1}^\pi(x) + V_{\theta_2}^\pi(x))$; the baselines use a single critic with the same architecture. Training is done following Section 4.2. Full training parameters for λ -Reachability and DPE are reported below.

Table 9: Safety-value learning hyperparameters. The main columns report the configuration used for the hardware-inference lineage; values that change for the simulation-inference lineage are listed in the last column. For λ -Reachability we additionally report ablations $\lambda \in \{0.99, 0.95, 0.50, 0\}$ in Section 4.4; the value shown here is the default ($\lambda=0.99$) used in all main results.

Hyperparameter	λ -Reachability	DPE	Sim-inference override
Critic ensemble	2 (clipped double- Q)	1	—
Horizon discount λ	0.99 (main)	annealed 0.9 \rightarrow 0.99	—
Per-step survival δ	0.99	—	—
Absorption value v_{term}	-10^6	—	—
Max bootstrap horizon n_{max}	200	1 (one-step TD)	—
Hidden dims, activation	[256, 256], ReLU	[256, 256], ReLU	—
Optimiser, learning rate α	Adam, 10^{-3}	Adam, 10^{-3}	—
Batch size B	256	256	—
Target Polyak rate τ	0.005	0.05	$\tau=0.05$ (λ -reach)
Target update period	every step	every 10 steps	every 10 steps (λ -reach)
Loss	regression + lower-bound hinge + monotonicity hinge + sign BCE ($\alpha_{\text{bce}}=5$); weights (1, 1, 1, 1)	MSE on ($1-\lambda$) ℓ + $\lambda \max(\ell, V^-(x'))$	hinge / BCE weights $\rightarrow 0$
Total gradient steps	10 000	10 000	2 000
Evaluation cadence	every 500 steps	every 500 steps	—
Random seed	0	0	—

C.4 Safety Value Inference

Simulation inference is performed by applying the learned V^π to the same environments on which the rollout policy was trained, and computing metrics according to Section 4.3. For hardware inference, we collect real data from policy rollouts with artificially generated disturbances. To record observations for G1COLLISION, we use an Optitrack motion capture system to stream the poses of both the humanoid base and a ball, which serves as the dynamic obstacle. The relative position and velocity of the ball in the humanoid base frame are computed online as part of the observation for the safety value function. The safety values are applied to the collected trajectories and evaluated against labeled safety signals following Section 4.3.

D Hardware Experiment Results

In this section, we present additional hardware experimental results on G1FLAT and G1COLLISION, including video screenshots and plots of the safety signal ℓ and the inferred safety value V^π . In each plot, we mark the timestamp of the external events that perturb the robot towards unsafe regions and observe the first timestamp at which λ -Reachability and the DPE baseline predict non-recoverable states, and the first timestamp of actual unsafe events. It is evident that λ outperforms the baseline via earlier warning and more accurate value prediction.

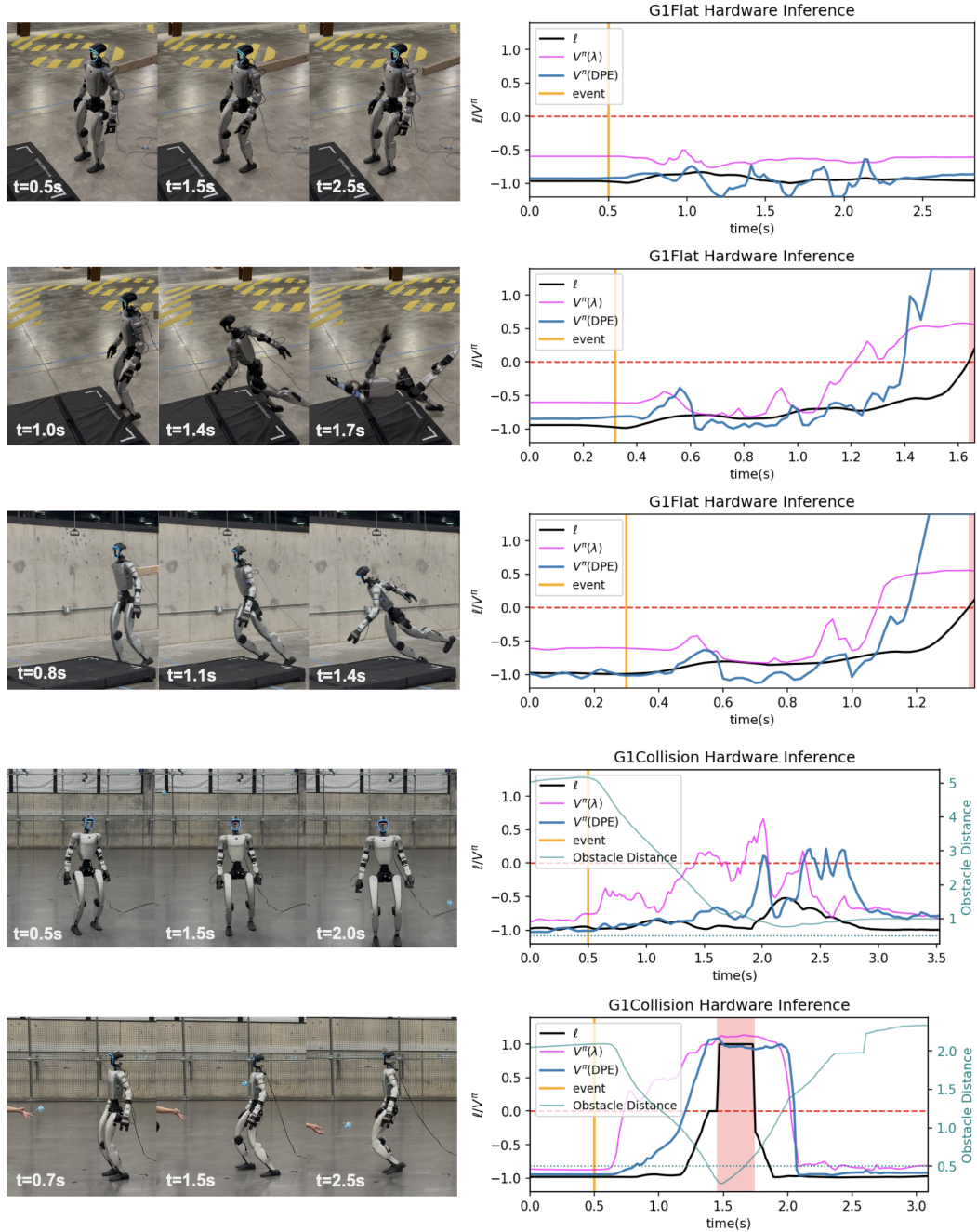


Figure 4: Additional hardware experiment results.